Stromal-derived NRG1 enables oncogenic KRAS bypass in pancreas cancer

Jincheng Han,[1] Jiaqian Xu,[2] Yonghong Liu,[1] Shaoheng Liang,[3,4] Kyle A. LaBella,[1] Deepavali Chakravarti,[1] Denise J. Spring,[1] Yan Xia,[1] and Ronald A. DePinho[1]

[1]Department of Cancer Biology, The University of Texas MD Anderson Cancer Center, Houston, Texas 77030 USA; [2]Department of Cancer Systems Imaging, Division of Diagnostic Imaging, The University of Texas MD Anderson Cancer Center, Houston, Texas 77030 USA; [3]Department of Bioinformatics and Computational Biology, The University of Texas MD Anderson Cancer Center, Houston, Texas 77030 USA

Activating KRAS mutations (KRAS*) in pancreatic ductal adenocarcinoma (PDAC) drive anabolic metabolism and support tumor maintenance. KRAS* inhibitors show initial antitumor activity followed by recurrence due to cancer cell-intrinsic and immune-mediated paracrine mechanisms. Here, we explored the potential role of cancer-associated fibroblasts (CAFs) in enabling KRAS* bypass and identified CAF-derived NRG1 activation of cancer cell ERBB2 and ERBB3 receptor tyrosine kinases as a mechanism by which KRAS*-independent growth is supported. Genetic extinction or pharmacological inhibition of KRAS* resulted in up-regulation of ERBB2 and ERBB3 expression in human and murine models, which prompted cancer cell utilization of CAF-derived NRG1 as a survival factor. Genetic depletion or pharmacological inhibition of ERBB2/3 or NRG1 abolished KRAS* bypass and synergized with $KRAS^{G12D}$ inhibitors in combination treatments in mouse and human PDAC models. Thus, we found that CAFs can contribute to KRAS* inhibitor therapy resistance via paracrine mechanisms, providing an actionable therapeutic strategy to improve the effectiveness of KRAS* inhibitors in PDAC patients.

[*Keywords*: pancreas cancer; tumor microenvironment; oncogenic KRAS bypass; receptor tyrosine kinase; cancer-associated fibroblasts; NRG1; ERBB3]

Supplemental material is available for this article.

Received August 8, 2023; revised version accepted September 13, 2023.

Pancreatic ductal adenocarcinoma (PDAC) is a highly lethal cancer with limited therapeutic options. Oncogenic mutations in KRAS (KRAS*) are nearly universal and drive tumor initiation and maintenance via activation of anabolic metabolism and suppression of antitumor immunity (Ying et al. 2012; Ischenko et al. 2021). The pivotal role of KRAS* in PDAC and other cancers has motivated the development of small molecules including covalent KRAS* inhibitors AMG510 and MRTX849 (Canon et al. 2019; Hallin et al. 2020), which specifically target the rare $KRAS^{G12C}$ allele; emerging inhibitors such as MRTX1133 (Hallin et al. 2022; Wang et al. 2022), which targets the more common $KRAS^{G12D}$ allele; and pan-KRAS inhibitor BI-2865, which prevents activation of KRAS and a broad range of KRAS mutants (Kim et al. 2023). Additional strategies to target KRAS* include exosome-mediated delivery of RNAi (Kamerkar et al. 2017).

Genetic extinction or pharmacological inhibition of KRAS* or its signaling surrogate, MEK, is associated with antitumor responses followed by tumor regrowth in both preclinical models and patients. In preclinical models, cancer cell-intrinsic resistance mechanisms include oncogene (KRAS or BRAF) amplification (Little et al. 2011), KRAS*/$KRAS^{WT}$ allelic imbalance and dimerization (Burgess et al. 2017; Ambrogio et al. 2018), mTORC signaling (Brown et al. 2020), YAP1 amplification and activation (Kapoor et al. 2014), RTK activation (Pettazzoni et al. 2015), epidermal growth factor receptor (EGFR)- and aurora kinase-mediated nonuniform adaptation of $KRAS^{G12C}$ (Xue et al. 2020), and PI3K-depedent MAPK signaling activation (Muzumdar et al. 2017). In addition, preclinical models have identified host-derived paracrine resistance mechanisms involving immune cells. Specifically, KRAS* inhibition results in up-regulation of HDAC5, leading to increased CCL2/CCL7 expression, which in turn recruits TGFβ-expressing macrophages, enabling Smad4-dependent survival of cancer cells (Hou et al. 2020). In PDAC patients treated with

[4]Present address: Department of Computational Biology, School of Computer Science, Carnegie Mellon University, Pittsburgh, PA 15213, USA.
Corresponding author: rdepinho@mdanderson.org
Article published online ahead of print. Article and publication date are online at http://www.genesdev.org/cgi/doi/10.1101/gad.351037.123.

$KRAS^{G12C}$ inhibitor, resistance mechanisms align well with insights derived from preclinical models, showing the emergence of alternative mutation or amplification of KRAS* as well as amplification, activating mutations, and oncogenic fusions of RTK/RAS/MAPK/PI3K pathway components (Awad et al. 2021; Tanaka et al. 2021).

Our inducible KRAS* PDAC model established that KRAS* is an essential tumor maintenance gene, though some mice can experience tumor recurrence involving mechanisms that enable KRAS*-independent growth (Ying et al. 2012; Kapoor et al. 2014; Hou et al. 2020). Specifically, these KRAS* bypass mechanisms involved cancer cell-intrinsic events such as YAP amplification and activation or RTK activation (Kapoor et al. 2014; Pettazzoni et al. 2015) as well as immune cell-mediated growth factor support of cancer cells via TGFβ activation of Smad3/4 survival signaling (Hou et al. 2020). Given this nonautonomous immune cell-mediated KRAS* bypass mechanism, coupled with the preponderance of CAFs in PDAC, we considered the possibility that CAFs could produce growth factors capable of bringing tumor recurrence upon KRAS* extinction in our model. Of relevance, NRG1 is normally expressed in the stroma, while its receptor, ERBB2/3, is expressed in cancer cells. In $KRAS^{WT}$ PDAC, the presence of NRG1 fusions also belied a potential NRG1–KRAS epistatic relationship (Heining et al. 2018; Topham et al. 2022). In this study, KRAS* inhibitor treatment resulted in dramatically increased expression of ERBB2/3 receptor tyrosine kinases in human and mouse models of PDAC. Biochemical and gain/loss-of-function studies established that NRG1 activation of ERBB2/3 enables escape from KRAS* inhibition. Anti-NRG1 or anti-ERBB2 antibody administration, together with KRAS* inhibitor treatment, resulted in more sustained antitumor responses and increased survival. These findings provide an actionable cotargeting strategy to enhance the effectiveness of KRAS* inhibitors in PDAC patients.

Results

CAF-secreted factors enable KRAS-independent growth of cancer cells*

To explore the role of CAFs in modulating the response to targeted KRAS* therapies, flow cytometry was used to isolate primary $CD45^-$, GFP^-, $CD31^-$, and $PDPN^+$ CAFs from tumors (Supplemental Fig. S1A) of the iKPC PDAC model, which is engineered with doxycycline (dox)-inducible $Kras^{G12D}$, conditional null *p53*, and *Ptf1a*-Cre alleles (Ying et al. 2012). The iKPC model generates PDAC tumors with GFP^+ cancer cells and GFP^- stroma that allow rapid and faithful tracing of cell origin. Two primary CAF cultures were generated from two iKPC tumors and designated as pCAF1 and pCAF2. Conditioned media (CM) from these cultures was used to assess its capacity to support in vitro growth of iKPC cancer cells in the presence or absence of dox or in the presence of dox plus 100 nM $KRAS^{G12D}$ inhibitor (MRTX1133). In both 2D and 3D Matrigel cultures, pCAF1 or pCAF2 CM supplementation produced a modest but significant increase in iKPC cell number and diameter under *Kras** on and off conditions (Fig. 1A–C). Given the limited quantity and proliferative capacity of primary CAFs for in-depth biochemical analyses and in vivo studies, a spontaneously immortalized cell line was generated from the primary pCAF1 culture and designated as CAF1, which exhibited fibroblast morphology, was negative for E-cadherin and $KRAS^{G12D}$ expression and positive for CAF marker expression (PDPN, PDGFRB, vimentin, and αSMA), and expressed myofibroblast marker genes as determined by RNA-seq (Supplemental Fig. S1B–D). Moreover, CAF1 CM demonstrated in vitro rescue activity comparable with that of its parental pCAF1 CM (Fig. 1A–C; Supplemental Fig. S1E,F).

To assess the capacity of these CAF cultures to support KRAS*-independent growth in vivo, nude mice without dox supplementation (*Kras** off) were injected with 1×10^6 luciferase-expressing iKPC cancer cells (iKPC1-luc or iKPC2-luc) or coinjected with 1×10^6 cells of either pCAF1 (less than three passages) or CAF1 cell lines plus either iKPC1 or iKPC2 cell lines. In separate experiments, pCAF1 or CAF1 cells failed to generate tumors (Supplemental Fig. S1H). While iKPC cancer cells did not generate tumors, iKPC + pCAF1 and iKPC + CAF1 coinjections exhibited tumor growth, as evidenced by increased bioluminescence signal compared with iKPC-luc injection alone (Fig. 1D,E). Tumor histology and GFP staining confirmed the presence of viable cancer cells without $iKras^{G12D}$ transgene expression within the tissue mass at the injection site (iKPC1-luc + CAF1) (Fig. 1F).

To explore the nature of CAF1 CM activity, the CM was subjected either to heat inactivation (10 min at 95°C; "CM-HI") to evaluate the role of proteins or to ultrafiltration (30- or 100-kDa molecular weight cutoff [MWCO]; "CM-30kFL" or "CM-100kFL") to determine the molecular weight range of the active substance(s). CAF1 CM Kras*-independent growth-sustaining activity was detected in the CAF1 CM-100k flowthrough but not CAF1 CM-HI or CAF1 CM-30k flowthrough (Fig. 1G; Supplemental Fig. S1G). Together, these data suggest that the CAF-derived growth-sustaining activity is mediated by protein (s), rather than metabolite(s), with a molecular weight range of 30–100 kDa.

To further define the putative CAF-secreted factor(s), we first assessed CM-directed modulation of KRAS*-relevant signaling surrogates in iKPC cancer cells. To that end, 24-h serum-free CM of pCAF1, pCAF2, and CAF1 cell cultures was subjected to ultrafiltration to remove metabolites and dialyzed to 10× concentration to produce CAF-derived protein concentrate (designated as CAF-pro); heat-inactivated (HI) CAF-pro served as a negative control (Fig. 1H). As a first step, we evaluated the capacity of CAF1-pro reconstituted to 1× concentration to activate the KRAS*-relevant signaling molecules AKT and ERK in iKPC cancer cells. Indeed, pCAF1-pro, pCAF2-pro, and CAF1-pro treatment of dox off (*Kras** off) iKPC cells showed robust and sustained AKT (pAKT-S473) and transient ERK (pERK activation without inducing re-expression of $KRAS^{G12D}$) (Fig. 1I). These patterns prompted us to consider that CAF-secreted factor(s) might activate

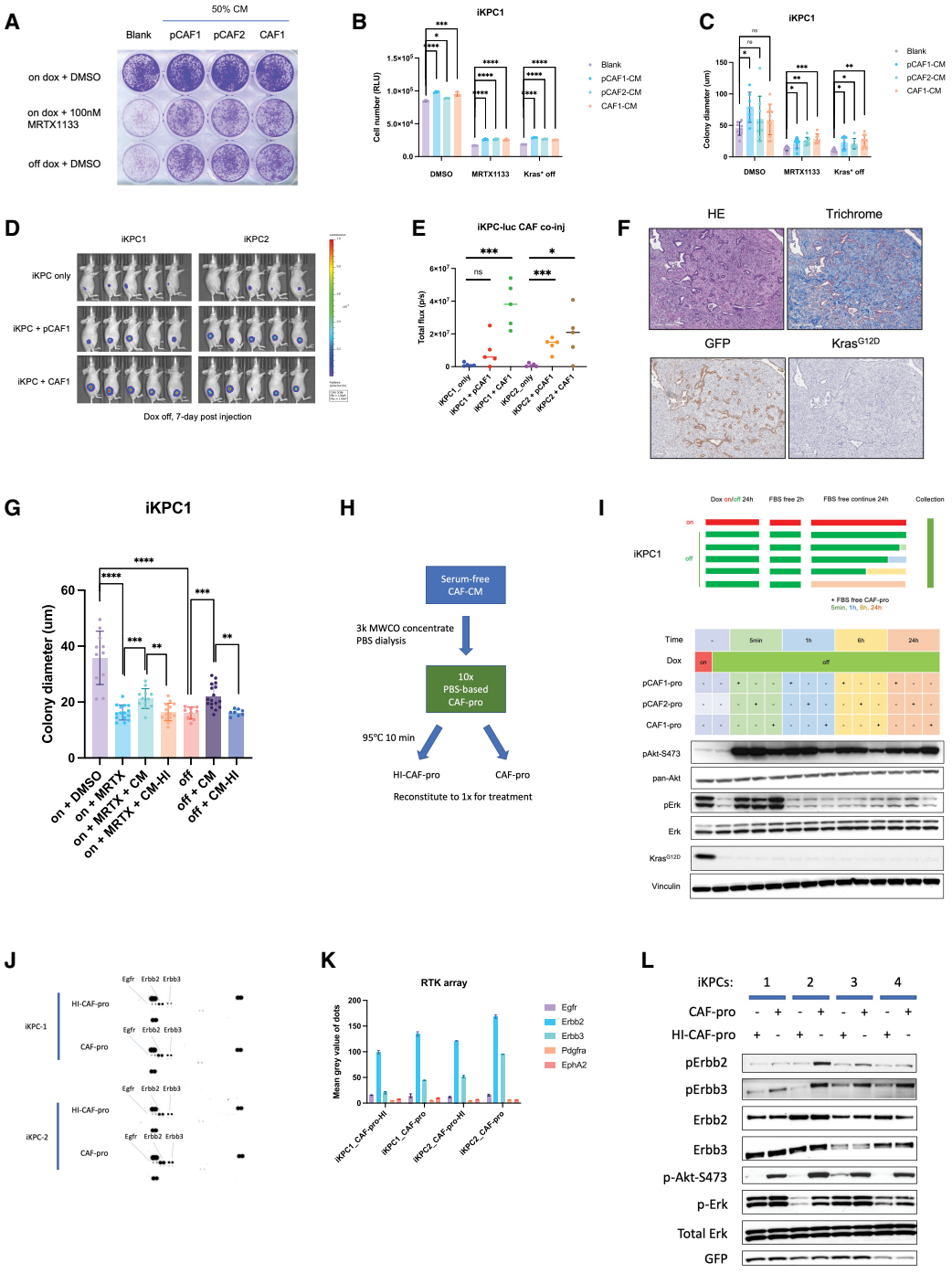

Figure 1. Cancer-associated fibroblasts promote resistance to KRAS* extinction in a PDAC model. (*A*) Crystal violet staining of iKPC1 cell colony formation assay, with Kras* on (on dox), MRTX1133, or Kras* off (off dox). The presence of 50% conditional medium from pCAF1, pCAF2, or CAF1 significantly increased the capacity of cell growth 4 d after treatment. (*B*) Measurement of cell viability using Celltiter-Glo in the same settings as in *A* 4 d after treatment. (*C*) Measurement of colony diameter of iKPC1 in Matrigel culturing assay in the same settings as in *A* 7 d after treatment. (*D*) Luciferase image of mice injected with 1×10^6 iKPC1-luc cells alone, iKPC2-luc cells alone, or iKPC1-luc or iKPC2-luc cells together with 1×10^6 pCAF1 or CAF1 cells 7 d after injection. Coinjection of iKPC and CAFs significantly increased KRAS*-independent growth. (*E*) Quantification of luciferase signal from *D*. (*F*) Histology (HE, trichome, GFP, and KRASG12D staining) of tissue mass from iKPC + CAF1 injection from *D*. (*G*) Measurement of colony diameter of iKPC1 in Matrigel culturing assay 7 d after treatment with the indicated condition and treatment. (DMSO) Dox on with DMSO, (MRTX) dox on with 100 nM MRTX1133, (Kras* off) dox off with DMSO, (CM) the presence of 50% CAF-CM in culture, (CM-HI) the presence of 50% heat-inactivated CAF-CM in culture. (*H*) Summary of the strategy for isolating CAF-secreted protein (CAF-pro). (*I*) Experimental settings and Western blot analysis of iKPC1 cells at the indicated time points after adding CAF-pro. (*J*) RTK array analysis of two iKPC cell lines after 5 min of CAF-pro or heat-inactivated CAF-pro (HI-CAF-pro) treatment. (*K*) Quantification of *J*. (*L*) Confirming ERBB2, ERBB3, and AKT phosphorylation in four different iKPC cell lines. Data are represented as mean ± SD for *B*, *C*, and *G*, and mean only for *E*. For *B*, *C*, *E*, and *G*, Student's *t*-test was performed to calculate statistical values.

receptor tyrosine kinases (RTKs). Subsequent RTK arrays revealed specific activation of pERBB2 and pERBB3 within 5 min of CAF1-pro, but not HI-CAF1-pro, treatment (Fig. 1J,K). Four independently derived iKPC cell lines confirmed consistent CAF1-pro-induced activation of pERBB2, pERBB3, and AKT (Fig. 1L). Together, these findings raised the possibility that CAF-secreted factors activate signaling pathways to enable KRAS*-independent PDAC growth.

Activation of NRG1–ERBB2/3 signaling enables KRAS bypass*

NRG1 is the only known ligand of the ERBB2/ERBB3 RTK heterodimer in which ERBB3 binds to NRG1, and ERBB2 possesses tyrosine kinase activity to engage downstream signaling (Hynes and Lane 2005; Baselga and Swain 2009). To validate CAFs as the source of NRG1, we conducted a series of studies. First, Western blot analysis showed abundant NRG1 expression in primary CAFs and CAF1 compared with negligible levels in iKPC cells; the specificity of the NRG1 band was confirmed by the reduced signal observed in CAF1 with gene-edited knockout of *Nrg1* and the presence of robust signal of ectopically expressed mouse NRG1 in iKPC1 cells and human NRG1 in AsPC1 cells (Fig. 2A). Second, in iKPC PDAC tumors, RNA in situ hybridization detected *Nrg1* transcripts in PDPN$^+$ cells (Fig. 2B; Supplemental Fig. S2A). Third, in iKPC tumors, RT-qPCR analysis showed higher *Nrg1* expression in PDPN$^+$-sorted CAFs compared with GFP$^+$-sorted iKPC cancer cells (Fig. 2C); similarly, RT-qPCR analysis of purified CAF subtypes documented *Nrg1* expression in all subtypes with slightly higher expression in myofibroblasts (myCAFs) and antigen-presenting fibroblasts (apCAFs) compared with inflammatory fibroblasts (iCAFs) (Supplemental Fig. S2B,C). In human PDAC tumors, *NRG1* mRNA levels were highly correlated with the CAF markers PDPN and ACTA2 and negatively correlated with the cancer cell marker KRT19 (Supplemental Fig. S2D).

To validate the role of NRG1–ERBB2/3 signaling in sustaining KRAS*-independent growth, three independent iKPC cell lines (iKPC1–3) were subjected to gene editing to generate multiple subclones null for *Erbb2* ($n = 2$ for each iKPC cell line), *Erbb3* ($n = 1$ for each iKPC cell line), or both ($n = 2$ for each iKPC cell line). The three iKPC parental lines and a derivative KO subclone were seeded into Matrigel with either dox, dox + 100 nM MRTX1133, or no dox. CAF1-pro or recombinant mouse (rm) NRG1 was added to the cultures, and colony diameters were measured at 7 d. Addition of CAF-pro or rmNRG1 showed robust growth of dox off or dox + MTRX1133 in all three parental iKPC cell lines but no growth for their derivative iKPC cells null for ERBB2 and/or ERBB3 (Fig. 2D; Supplemental Fig. S2E). Correspondingly, genetic deletion of *Erbb2* and/or *Erbb3* greatly abrogated CAF-pro- or rmNRG1-induced activation of AKT while mildly and variably attenuating activation of ERK across different cell lines (Fig. 2E; Supplemental Fig. S2F). These findings, together with the observation from Figure 1I showing that CAF-pro induced pAKT activation, align with previous work establishing that ERBB3-mediated activation predominantly stimulates the PI3K–AKT pathway due to its inherent ability to bind directly with the p85 subunit of PI3K (Hynes and Lane 2005; Baselga and Swain 2009). Reintroduction of ERBB3 in ERBB3-KO cells restored their ability to activate AKT (Fig. 2F).

To confirm that CAF CM-derived NRG1 activates AKT, we stimulated the iKPC1 cells with CAF1-CM that had been incubated with mouse IgG (control) or anti-NRG1 antibody YW538.24.71 (NRG1-depleted) or with CM derived from CAF1-*sgNrg1* (Fig. 2G). The presence of YW538.24.71 or genetic deletion of *Nrg1* in CAF1 eliminated the CAF-pro-induced AKT activation. Consistent with these murine findings, human PDAC cell lines AsPC1, Panc 05.04, and Panc 10.05 treated with human anti-ERBB2 antibody (pertuzumab) showed decreased activation of ERBB3, AKT, and ERK upon addition of CAF-pro or rmNRG1 (Fig. 2H; Supplemental Fig. S2G). Moreover, pertuzumab and YW538.24.71 abrogated the capacity of both CAF1-pro and rmNRG1 to rescue AsPC1 growth in the setting of MRTX1133 treatment (Fig. 2I). To confirm the requirement of NRG1 in KRAS*-independent growth, we coinjected 1×10^6 freshly isolated pCAF3 cells from an iKPC tumor (less than three passages) or CAF1 cells together with 1×10^6 iKPC1-luc cells into nude mice; injections were conducted in the presence of mouse IgG1 or YW538.24.71 or nontargeted control and NRG1-null CAF1 cells with iKPC1-luc. The neutralization or the genetic deletion of NRG1 in CAF1 greatly impaired the capacityof CAF1 to support KRAS*-independent tumor growth, as evidenced by reduced luciferase signal. (Fig. 2J, K; Supplemental Fig. S2H). Predictably, depletion of NRG1 in CAF1 also greatly reduced their capacity to support KRAS*-independent tumor mass formation (Supplemental Fig. S2I,J). Together, these data suggest that CAF-mediated NRG1-induced ERBB2/3 activation facilitates KRAS* bypass of PDAC cancer cells.

The CAF-pro-mediated activation of ERBB2/3 prompted us to analyze the essentiality of NRG1 in driving KRAS*-independent growth. To that end, NRG1 expression was enforced in parental iKPC1 cells, their derivative cells null for ERBB3 (iKPC1-ERBB3-KO), and iKPC1-ERBB3-KO cells rescued with *Erbb3*-ORF expression vector (iKPC1-ERBB3-res) (Supplemental Fig. S3A). Enforced NRG1 expression activated AKT and supported KRAS*-independent growth in Matrigel cultures of iKPC1 and iKPC1-ERBB3-rescued cells but not in iKPC1-ERBB3-KO cells (Supplemental Fig. S3B,C). Moreover, NRG1-expressing iKPC1 cells but not control iKPC1 cells (both *Kras** off) rapidly generated tumors with classical PDAC histology with activation of ERBB3, ERK, and AKT and expression of NRG1 in cancer cells (Supplemental Fig. S3D, E). Equivalent findings were generated with NRG1-expressing versus parental human AsPC1 cells treated with MRTX1133 (Supplemental Fig. S3F,G). Two weeks of MRTX1133 treatment provided a significant survival benefit for mice injected with AsPC1 cells, but mice injected with NRG1-expressing AsPC1 cells succumbed rapidly from highly proliferative tumors showing high pERBB3 and Ki67 signals (Supplemental Fig. S3H,I).

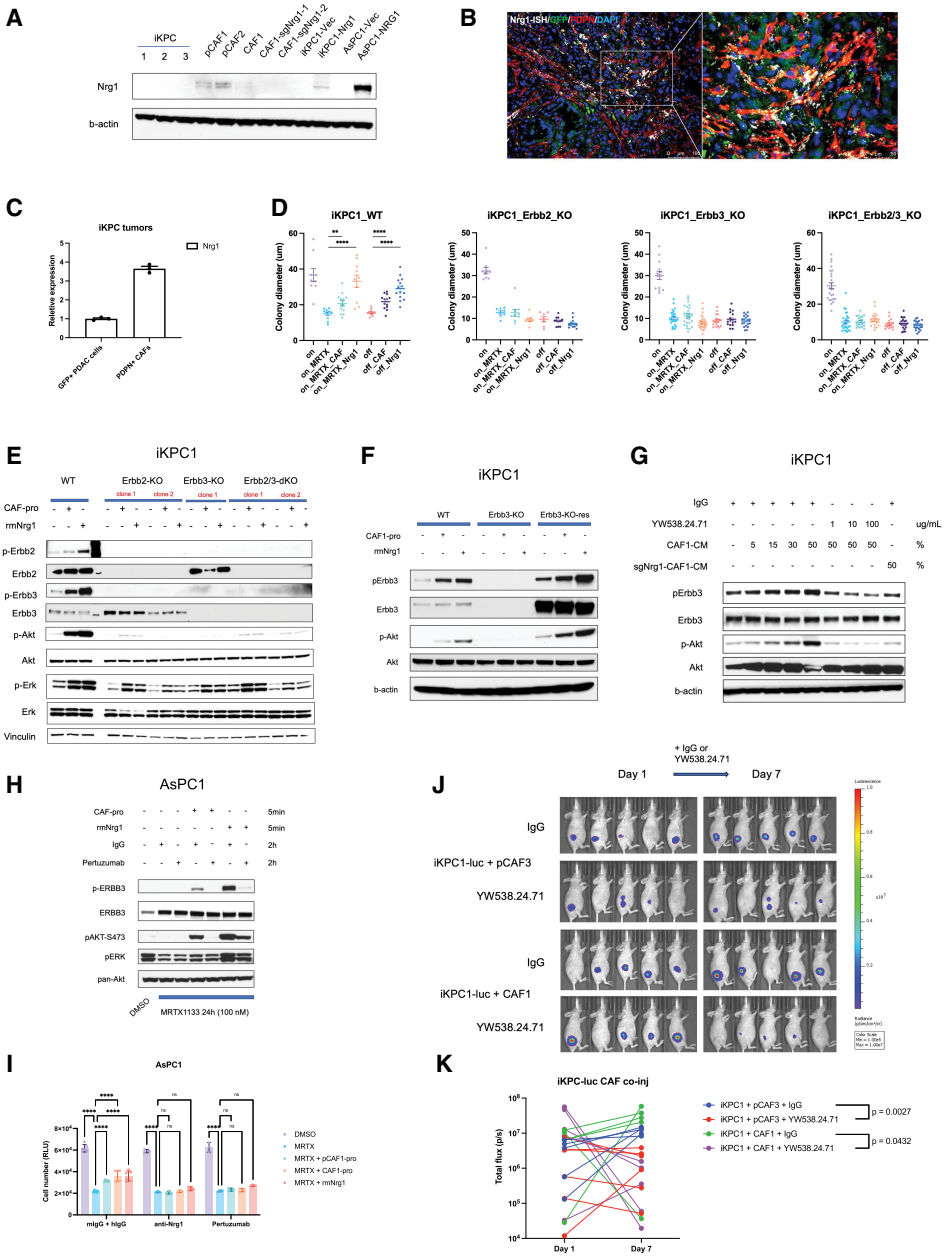

Figure 2. Paracrine Nrg1–Erbb2/3 signaling activation confers KRAS* resistance. (*A*) Western blot of NRG1 protein levels in various cell lines. (*B*) Multiplexed RNAscope immunofluorescence staining of iKPC tumor with NRG1-specific RNA probe (white), GFP (green), PDPN (red), and DAPI (blue). (*C*) qPCR results of Nrg1 on flow cytometry-sorted GFP$^+$ PDAC cells or PDPN$^+$ CAFs from iKPC GEM tumors. Two independent tumors were pooled together for dissociation. (*D*) Measurement of colony diameter of iKPC1 in 3D Matrigel culturing assay with the indicated treatment for 7 d. (on) Kras* on with dox, (off) Kras* off without dox, (MRTX) 100 nM MRTX1133 treatment, (CAF) the presence of CAF1-pro in culture, (NRG1) the presence of 10 ng/mL rmNRG1 in culture. Data are represented as mean ± SEM; Student's *t*-test. (*E*) Western blot of the indicated iKPC1 knockout clones Kras* off for 48 h and serum-starved for 2 h prior to 5-min stimulation of the indicated treatments (CAF1-pro or 10 ng/mL rmNRG1). (*F*) Western blot of the indicated iKPC1 ERBB3 knockout or rescued clones K Kras* off for 48 h and serum-starved for 2 h prior to 5-min stimulation of the indicated treatments (CAF1-pro or 10 ng/mL rmNRG1). (*G*) Western blot of iKPC1 cells with 48 h of K Kras* off and 2 h of serum starvation prior to 5-min stimulation of the indicated treatments (CAF1-pro cells were preincubated with 100 µg/mL mouse IgG or the indicated concentration of NRG1 neutralization antibody YW538.24.71 for 1 h at 37°C). (*H*) Western blot of AsPC1, DMSO, or 100 nM MRTX1133 treatment for 24 h and serum starvation for 2 h with the presence of 10 µg/mL control human IgG or 10 µg/mL pertuzumab prior to 5-min stimulation of the indicated treatments (CAF-pro, 10 ng/mL rmNRG1, or CAF-sgNrg1-pro). (*I*) Cell viability assay with AsPC1 with the indicated treatment for 4 d. (MRTX) Treated with 100 nM MRTX1133 (with pCAF1-pro, CAF1-pro, or 10 ng/mL rmNRG1), (mIgG + hIgG) treated with 10 µg/mL control mouse IgG and 10 µg/mL control human IgG, (anti-NRG1) the presence of 10 µg/mL YW538.24.71, (pertuzumab) the presence of 10 µg/mL pertuzumab. Data are represented as mean ± SD; two-way ANOVA. (*J*) Luciferase assay of iKPC1-luc cells coinjected with pCAF3 or CAF1. One day after cell implantation, luciferase signal was measured to acquire the initial value of luciferase activity, and IgG or YW538.24.71 was given at a dose of 25 mg/kg. Luciferase signal was acquired again at 7 d after implantation. (*K*) Quantification of luciferase signal from *J*. Paired multiple *t*-test at day 7.

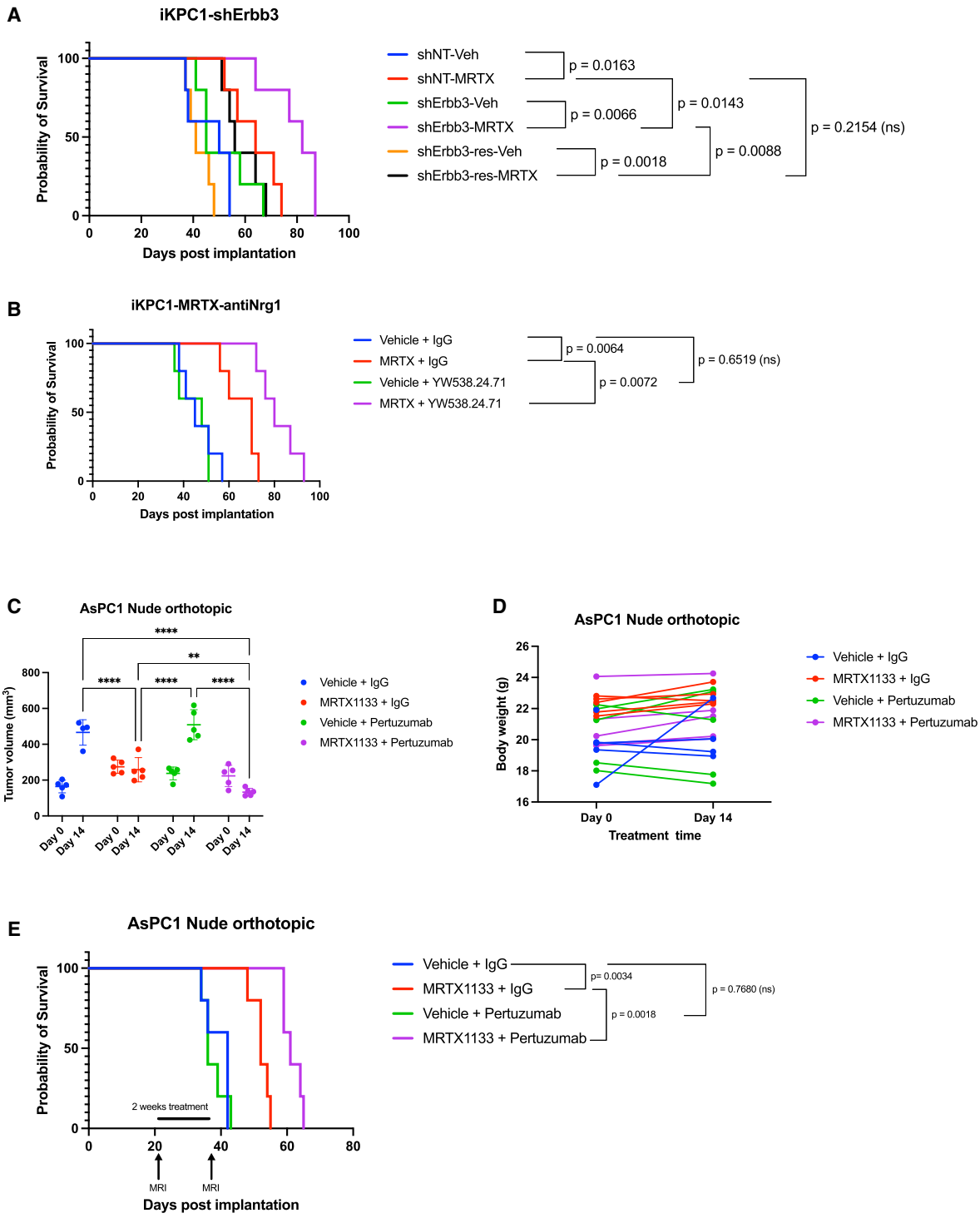

Figure 3. NRG1–ERBB signaling inhibition synergizes with MRTX1133. (*A*) Kaplan–Meier survival analysis of iKPC1 with the indicated shRNA and treatment. (shNT) Nontargeting shRNA, (shErbb3) shRNA targeting Erbb3, (shErbb3-res) shRNA targeting Erbb3 with hairpin-resistant Erbb3 ORF. $n = 5$ per group. (Veh) Vehicle treatment, (MRTX) MRTX1133 treatment (30 mg/kg body weight, b.i.d.). (*B*) The Kaplan–Meier survival analysis of iKPC1 with the indicated treatment. (Veh) Vehicle treatment, (MRTX) MRTX1133 treatment (30 mg/kg body weight, b.i.d.). (IgG mouse IgG2a) and YW538.24.71 (anti-NRG1) were administered weekly at 25 mg/kg body weight. $n = 5$ per group. (*C*) Tumor volume of AsPC1 orthotopic xenograft model determined by MRI before and after treatment. (Vehicle) Vehicle treatment, (MRTX1133) MRTX1133 treatment (30 mg/kg body weight, two times a day [b.i.d.]). IgG (human IgG1) and pertuzumab (anti-HER2) were administered weekly as follows: first dose of 12 mg/kg body weight and second dose of 6 mg/kg body weight. $n = 5$ per group. (*D*) Body weight measurement of mice before and after treatment in *C*. (*E*) The Kaplan–Meier survival analysis of mice from *C*.

Together, these findings implicate the NRG1–ERBB3 axis as a potential KRAS* bypass mechanism.

Targeting the NRG1–ERBB2/3 axis enhances KRAS inhibitor therapy*

Human PDAC (TCGA-PAAD) transcriptome analysis showed prominent expression of ERBB2 and ERBB3 on cancer cells relative to other growth factor receptors (Supplemental Fig. S4A–C). Moreover, consistent with prior studies showing that MEK inhibition up-regulates ERBB2/3 expression (Sun et al. 2014) and that MRTX1133 treatment up-regulates ERBB2 expression (Gulay et al. 2023), analysis of published xenograft and cell line RNA-seq data (Hallin et al. 2022) showed consistent increases in ERBB2/3 expression in diverse $KRAS^{G12D}$ models including PDAC (Supplemental Fig. S4D,E). Notably, ERBB2 and ERBB3 were the two most differentially up-regulated RTKs upon *Kras** extinction in iKPC1–3 cell lines (Supplemental Fig. S4F), and MRTX1133 treatment induced dramatic up-regulation of ERBB2 and ERBB3 at the protein level in mouse iKPC cell lines, mouse iKPC tumors, human AsPC1 cell culture, and orthotopic transplanted tumors (Supplemental Fig. S4G–I). Together, these findings point to an intimate link between KRAS* and ERBB2/3 survival signaling in PDAC.

Next, to functionally evaluate the role of the NRG1–ERBB2/3 axis in the antitumor response to MRTX1133 therapy, we generated iKPC1 cells expressing nontargeting shRNA (shNT), *shErbb3*, or *shErbb3* plus hairpin-resistant *Erbb3* (Supplemental Fig. S5A,B). These cells were orthotopically injected into B6 mice on dox and assessed by MRI at 14 d after implantation for comparable tumor sizes (~100 mm^3) across all three groups (Supplemental Fig. S5C). Tumor-bearing mice randomized and treated with vehicle or MRTX1133 two times a day (b.i.d.) for 2 wk showed improved survival in the iKPC1-*shErbb3* group relative to iKPC1 or iKPC1-ERBB3 rescue controls (Fig. 3A). In parallel, the impact of MRTX1133 treatment was assessed in the presence or absence of anti-NRG1 antibody treatment. Specifically, MRI-documented iKPC1 tumor-bearing mice were randomized and enlisted into four 2-wk treatment groups: vehicle + IgG, vehicle + anti-NRG1, MRTX1133 + IgG, and MRTX1133 + anti-NRG1. As observed previously, anti-NRG1 antibody treatment was associated with hyperactivity and tremors (Dominguez et al. 2018). While anti-NRG1 antibody treatment alone did not yield a survival advantage, combined anti-NRG1 antibody and MRTX1133 treatment increased survival over MRTX1133 treatment alone (Fig. 3B). Given the toxicity of anti-NRG1 treatment, we also targeted ERBB2/3 in the context of MRTX1133 treatment. To that end, we used the clinically approved anti-ERBB2 antibody pertuzumab alone or in combination with MRTX1133 in nude mice orthotopically transplanted with AsPC1 cells. MRI-documented tumor-bearing mice were randomized and treated for 2 wk with 30 mg/kg MRTX1133 (b.i.d.) and/or pertuzumab (12 mg/kg the first week and then 6 mg/kg the second week). While MRTX1133 monotherapy stabilized AsPC1 tumor growth, combined MRTX1133 plus pertuzumab treatment produced tumor regression and improved overall survival without significant body weight loss (Fig. 3C–E). Histological examination of tumors at 14 d after treatment revealed decreased pERBB3 and Ki67 signals relative to MRTX1133 monotherapy (Supplemental Fig. S5D). Together, these findings provide preclinical proof of concept in support for the clinical evaluation of combined therapies targeting KRAS* and ERBB2/3 in PDAC patients.

Discussion

In this study, exploration of the resistance mechanisms to KRAS* inhibition in PDAC identified a paracrine mechanism involving CAF-derived NRG1 activation of ERBB2/3–AKT signaling in cancer cells. Genetic or pharmacological disruption of this heterotypic signaling produced robust antitumor synergy with KRAS* inhibition in murine and human PDAC models, providing an actionable strategy to improve the clinical responses to KRAS* inhibitor therapy.

While RTK activation is an emergent theme in recurrent disease in the setting of KRAS* inhibitor therapy, the mechanism of RTK activation is not fully understood. Identification of NRG1 and its cellular source reveals for the first time the role of CAFs in supporting KRAS*-independent growth via activation of ERBB2/3, commonly expressed RTKs in PDAC cancer cells. Furthermore, it is worth noting that KRAS* inhibition is associated with further up-regulation of ERBB2/3, which may position cancer cells to exploit this signaling axis to enable survival and the acquisition of various resistance mechanisms such as activating mutations in KRAS* or various RTKs and YAP amplification, among other mechanisms as summarized above. In addition to CAFs, other stromal cells may serve as additional sources for NRG1, though our work verifies CAFs as a key source. Our work also establishes that AKT activation is a major downstream target of the NRG1–ERBB2/3 signaling axis, which prompts speculation that activating mutations in AKT may be expected in KRAS* inhibitor disease recurrence.

The physiological relevance of the NRG1–ERBB2/3 axis in the context of KRAS signaling is reinforced by the presence of NRG1 fusions in nearly 25% of $KRAS^{WT}$ PDAC (Heining et al. 2018; Topham et al. 2022), consistent with an epistatic relationship between NRG1–EBBR2/3 and KRAS*. In addition, our analyses show that ERBB2 and ERBB3 are two of the most abundant receptor kinases in PDAC cancer cells, further strengthening their importance in PDAC biology and KRAS* inhibitor bypass. In support of our finding, the multikinase inhibitor afatinib, which targets EGFR, ERBB2, and ERBB4, shows synergy with the KRAS* inhibitor MRTX1133 (Gulay et al. 2023). Using genetic deletion as well as targeted therapies, our work precisely identifies NRG1–ERBB2/3as the key target, which provides a clear clinical hypothesis for precision therapeutics.

Materials and methods

Transgenic mice

Mouse experiments were approved by MD Anderson Cancer Center's Institutional Animal Care and Use Committee (IACUC). iKPC mice were maintained in the C57BL/6 background harboring TetO_Lox-Stop-Lox-*Kras*^{G12D}, ROSA26-LSL-rtTA-IRES-GFP, p48-Cre, and Trp53L/+. Doxycycline (Takara 631311) was administered via ad lib water (2 mg/mL doxycycline, 40 mg/mL sucrose) at 4 wk of age to induce KRAS^{G12D} expression.

Cell implantation

Cell implantation was performed following standard protocols as previously described (Gulhati et al. 2023). In brief, C57BL/6 female mice aged 5–7 wk (Jackson Laboratory 000664) were anesthetized by isoflurane before orthotopic pancreas injection. Analgesic was administered before surgery (Buprenorphine ER, ZooPharm). The left abdomens of the mice were incised, with both the pancreas and spleen being extracted. iKPC cells (5×10^5 per 5 µL) mixed with 5 µL of Matrigel (Corning 354234) were injected into the tail of the pancreas via Hamilton syringe. Doxycycline was administered via ad lib water (2 mg/mL doxycycline, 40 mg/mL sucrose) 1 d before cell implantation.

The iKPC-CAF coinjection assay was performed subcutaneously on 3- to 4-wk-old female nude mice (Jackson Laboratory 002019). The iKPC cells used for coinjection experiments were transfected with the luciferase-mCherry reporter as previously described (Kapoor et al. 2014). After being washed in PBS, iKPC cells were resuspended in Opti-MEM (Gibco 31985062) before implantation. iKPC-luc cells only (10^6), CAFs only (10^6), or a mixture of iKPC-luc (10^6) and CAFs (10^6; total of 2×10^6) were resuspended with 50 µL of Opti-MEM and mixed with 50 µL of Matrigel, followed by subcutaneous implantation on the lower right flank or multiple injection as shown in Supplemental Figure S2G. All nude mouse implantation experiments were conducted without doxycycline to genetically extinguish KRAS* from iKPC cells.

Noninvasive mouse imaging

A 7T MRI (Bruker Biospin MRI Biospec USR70/30) was used to determine the size of orthotopic tumors. In brief, 30 axial slides, each with 0.75-mm thickness and a gap of 0.25 mm, were performed on each mouse. The tumor volume was calculated based on the sum of [(ROI area on each slide) × (0.75 mm)] + [(the average ROI area on the current and next slide) × (0.25 mm)], where ROI is the region of interest.

For bioluminescence imaging for subcutaneous tumors, mice were injected with 1.5 mg of D-Luciferin (Perkin Elmer 122799) intraperitoneally (100 µL) and imaged using an IVIS spectrum imaging system (Perkin Elmer) for 10 min following injection. Images were acquired and analyzed via Living Image 4.3 software (Perkin Elmer).

Flow cytometry sorting

iKPC tumors were processed by mouse tumor dissociation kit (Miltenyi Biotec 130-096-730) to obtain single-cell suspensions. Cell surface immunofluorescence staining was performed according to the protocol from BioLegend. In short, cells were incubated with TruStain FcX antibody (BioLegend 101320) for 10 min and then with the indicated labeled antibodies (see Supplemental Table S1) for 15 min on ice. Cells were washed, resuspended in staining buffer (1% FBS, 2 mM EDTA in PBS, filtered with 0.22-µm filters) with DAPI as a live/dead marker, and sorted by BD FACSAria sorter (BD Biosciences) at the Advanced Cytometry and Sorting Core Facility at MD Anderson Cancer Center.

Establishment and culture condition of cell lines

All cells were cultured in a humidified incubator at 37°C with 5% CO_2. GFP-positive iKPC cells were flow-sorted and cultured in DMEM + 10% Tet-approved FBS (Clontech [which now belongs to Takara] 631368) + penicillin–streptomycin (Gibco 15140122) with 1 µg/mL doxycycline (Takara 631311) in cell culture dishes (Falcon). For Matrigel-based 3D cell culture, 2000–5000 iKPC cells were suspended in Matrigel and plated in 24-well Nunclon Delta Surface plates (Thermo) using the same culture media as 2D culturing. Flow-sorted primary CAFs (GFP$^-$, CD45$^-$, CD31$^-$, and PDPN$^+$) were cultured in the same condition described above but without doxycycline, and the cells were cultured for less than three passages before conditioned media collection, coinjection, or Western blot analysis. To establish spontaneously immortalized CAF1, pCAF1 cells were cultured in cell culture dishes with the media changed every week until the cells overcame the initial growth stall in ~4 wk.

Cell viability assay

Cells were seeded into 96-well opaque assay plates (Corning 3603) for luminescence-based assay or regular 96-well culture plates (Corning or Greiner) with 100 µL of complete culture media. Viable cells were counted using Trypan blue exclusion at the beginning of experiments using Countess II (Thermo). On the second day after plating, 100 µL of culture media or conditioned media with the indicated concentration of treatment was added to make a total 200-µL volume. For luminescence-based assays, 150 µL of media was carefully removed and 50 µL of Celltiter-Glo (Promega G7571) was added for 10 min at room temperature after the indicated time of treatment. Signal was then obtained on a plate reader, and the negative control signal was defined using a well containing blank culture media. For crystal violet-based assays, cells were washed with PBS and incubated with 0.5% (w/v) crystal violet (Sigma) in 20% methanol for 10 min at room temperature. The plates were washed with tap water, dried thoroughly, and photographed. To quantify the cell viability, 200 µL of 100% methanol was added to each well to completely dissolve the crystal violet, and OD570 absorbance was determined using a microplate reader (BMG Labtech) to calculate relative cell viability.

Obtaining and processing conditioned media and CAF-derived protein concentrates

CAF cells were cultured in complete culture media until 90% confluency, the media was removed, and fresh media was added for 24 h to obtain CAF-CM. To obtain CAF-derived proteins, cells at 90% confluency were washed three times in PBS and cultured in blank DMEM for 24 h to obtain serum-free CAF-CM. The serum-free CAF-CM was filtered with 0.45-µm filters and concentrated to 1/10 of its original volume using 3-kDa MWCO ultrafiltration tubes (Millipore Sigma) to obtain CAF-pro. To obtain the flowthrough of CAF-CM, serum-free CAF-CM was processed in 30-kDa MWCO or 100-kDa MWCO ultrafiltration tubes, and the flowthrough was collected for the indicated experiments. To heat-inactivate CAF-CM or CAF-pro, media was incubated for 10 min at 95°C.

RNA extraction, qRT-PCR, and mRNA sequencing

To evaluate the KRAS*-regulated transcriptome, 50,000 iKPC cells were resuspended in 500 µL of Matrigel and plated in six-

well plates in the presence of complete culture medium and dox. Seventy-two hours later, the wells were washed with and soaked in PBS until the phenol red in the Matrigel completely disappeared and to remove any remaining dox. Next, the PBS was removed and complete culture medium with or without dox was added for another 48 h. To collect the cells, the Matrigel was disrupted by pipette in cold PBS and digested with 100 µg/mL Dispase II (Roche 04942078001) for 10 min at 37°C to obtain cell pellets.

RNA extraction from cell samples was performed using the RNA extraction kit (Qiagen 74034). RNA concentration was determined by the Nanodrop 2000 (Thermo Fisher Scientific). RNA samples were sent to BGI for RNA sequencing analysis (DNBseq PE150) or were otherwise reverse-transcribed for qRT-PCR analysis using 5× All-In-One RT master mix (abmGood G592) (see Supplemental Table S1 for primer sequences). The 7500 Fast real-time PCR system (Applied Biosystems) was used to perform qRT-PCR with SYBR Green PCR master mix (Applied Biosystems). Data were recorded by 7500 software v2.3 and analyzed by its default gene quantification method.

Antibodies, Western blot, immunohistochemistry, RNAscope, and multiplexed immunofluorescence staining

The following antibodies were used for Western blots and/or IHC: phospho-HER2/ErbB2 (Tyr1248; RRID AB_331725), HER2/ErbB2 (29D8; RRID AB_10692490), phospho-HER3/ErbB3 (Tyr1289; 21D3; RRID AB_2099709), HER3/ErbB3 (D22C5) XP (RRID AB_2721919), NRG1/Heregulin (RRID AB_1031011), p-AKT(S473) (RRID AB_2315049), AKT (RRID AB_1147620), p-p44/42 (pErk; RRID AB_2315112), p44/42 MAPK (Erk 1/2; RRID AB_390779), vinculin (RRID AB_477617), β-actin (RRID AB_476697), anti-mouse IgG (HRP-linked; RRID AB_330924), antirabbit IgG (HRP-linked; RRID AB_2099233), Ras (G12D mutant-specific; D8H7; RRID AB_2728748), GFP (D5.1; RRID AB_639257), anti-PDGFRβ (42G12; RRID AB_1269704), antipodoplanin/gp36 (RTD4E10; RRID AB_298718) anti-α-smooth muscle actin (RRID AB_11212646), vimentin (D21H3; RRID AB_10695459), E-cadherin (24E10; RRID AB_2066683), and Ki-67 (D3B5; RRID AB_2575902). For Western blot analysis, cell pellets were incubated in NP-40 lysis buffer (Research Products International N32000) for 20 min with the Halt protease inhibitor cocktail (Thermo 78430) and PhosSTOP (Roche 4906845001). The lysis was then centrifuged at maximum speed for 15 min, and the supernatants were isolated and quantified using DC protein assay kit (Bio-Rad 5000111). Equal amounts of total protein for each sample were used in each experiment.

For RTK array analyses, proteome profiler mouse phospho-RTK array kits (ARY014) were used. Cells were cultured in complete culture media without dox for 24 h and then starved in blank DMEM for 2 h before they were stimulated by the indicated treatment for 5 min.

For immunohistochemistry analyses, tissues were fixed in 4% PFA for 24 h and processed for embedding. Slides were deparaffinized in xylene and rehydrated in ethanol sequentially, and antigen retrieval was performed in citrus-based antigen unmasking solution (Vector Laboratories H-3300-250). Endogenous peroxidase activity was quenched by 0.3% hydrogen peroxide in 50% methanol for 30 min. Slides were blocked in rodent block M (Biocare Medical RBM961) and incubated with primary antibody diluted in antibody dilution buffer (Dako S080983-2). For primary antibody from rabbits, rabbit on rodent HRP polymer (Biocare Medical RMR622) was used. For primary antibody from Syrian hamsters, Biotin-SP (long spacer) AffiniPure goat anti-Syrian hamster IgG (H+L; Jackson Immunoresearch 107-065-142) was used, followed by VectaStain Elite ABC-HRP kit (Vector Laboratories PK-6100). DAB Quanto (Epredia TA125QHDX) was used to visualize antibody-specific signal, and the slides were counterstained with hematoxylin.

RNAscope for *Nrg1* was performed according to the ACD standard protocol using RNAscope Multiplex fluorescent reagent kit v2 (ACD 323100) and the probe 418181-C3. RNAscope 3-plex negative control probe (ACD 320871) was used to determine the unspecific bindings. After developing the *Nrg1*–RNA signal using TSA-Vivid-650 (Tocris), subsequent staining was performed using GFP antibody (rabbit on rodent HRP polymer + TSA-Vivid-520; Tocris) and PDPN antibody (biotin goat anti-Syrian hamster IgG + ABC-HRP + TSA-Vivid-570; Tocris). Peroxidase quenching was performed after each round of TSA development using HRP blocker provided in the RNAscope kit. The stained slides were mounted with antifade mounting medium with DAPI (Vector Laboratories H-1200-10) and imaged on a Leica DMi8 microscope.

Plasmid construction and gene knockdown, knockout, and overexpression

LentiORFs were purchased from Origene for mouse *Erbb2* (NM_001003817, MR227307), mouse *Erbb3* (NM_010153, MR227559), mouse *Nrg1* (NM_178591, MR226911L3), and human *NRG1* (NM_013956, RC220134). Except for mouse *Nrg1*, all ORFs were cloned into pLenti6.3/V5-DEST plasmid. Sanger sequencing was performed to verify the correct insertions. Empty vectors, pLenti-C-Myc-DDK-P2A-Puro for mouse *Nrg1* ORF, and XbaI-digested pLenti6.3/V5-DEST (removing the *ccdB* gene) for the other ORFs were used as controls. To express the ORFs in cells, lentiviruses containing the indicated vector controls or ORFs were made from 293T cells by cotransfecting psPAX2 (Addgene 12260) and pMD2.G (Addgene 12259), and the infected cells were selected with 2 µg/mL puromycin or 10 µg/mL blasticidin as per the plasmid resistance.

The knockout clones of iKPC1-3 and CAF1 were generated using PX458 plasmid (Addgene 48138). In brief, two PX458 plasmids (with different sgRNAs) targeting one gene or four PX458 plasmids targeting two genes (*Erbb2* and *Erbb3* double knockout) were transiently transfected into the target cells using Lipofectamine 3000 (Thermo L3000001) (see Supplemental Table S1 for sgRNA sequences). Forty-eight hours after transfection, single clones of GFP^+ cells were sorted into 96-well plates. To retain the heterogeneity of CAF1, all GFP^+ CAF1 cells were bulk-sorted into tubes, subsequently cultured, and tested for abrogated NRG1 expression. Nontargeting control (sgNT) transfected cells were bulk-sorted with GFP^+ signal as controls.

To preserve the heterogeneity and tumor formation capacity of iKPC1 in syngeneic transplantation, *Erbb3* knockdown was achieved by shRNA. In brief, pGIPZ shRNA constructs targeting *Erbb3* and nontargeting control were purchased from the Functional Genomics Core at MD Anderson Cancer Center (see Supplemental Table S1 for shRNA antisense sequences). The lentivirus was generated and the cells were infected and selected as described above. The rescue of shRNA-resistant *Erbb3* ORFs was generated by PCR using KAPA HIFI Hotstart Readymix (Roche KK2602) with the template (pLenti6.3/V5-Erbb3 plasmid described above) and the primers carrying silent mutations on the shRNA targeting region, followed by blunt ligation and Sanger sequencing.

Public data set analysis

Correlation data analysis between NRG1 and other markers was performed on cBioPortal using the TCGA-PAAD data set (Firehose Legacy). Expression data were downloaded, and the receptor

kinase list was obtained from Hugo Gene Nomenclature Committee (https://www.genenames.org). Pearson correlations between each receptor kinase expression were calculated against KRT19 expression in each patient, and the data were plotted by GraphPad Prism 9.

To analyze the expression of ERBB2 and ERBB3 in MRTX1133-treated cell lines and xenografts from (Hallin et al. (2022), GSE201412 data were downloaded and normalized in transcripts per million (TPM). The ERBB2 and ERBB3 expression levels in TPM from different groups were plotted by GraphPad Prism 9.

Recombinant proteins, therapeutic antibodies, and small molecule inhibitors

Recombinant mouse NRG1 (9875-NR) was purchased from R&D. YW538.24.71 was acquired from Genentech through an MTA request (ID OR-223620). Pertuzumab was obtained from Selleck (A2008). Mouse IgG2a and human IgG1 were purchased from BioXcell (BE0085 and BE0297). MRTX1133 was purchased from Chemitek (CT-MTX1133, lot 02). For in vitro culture, MRTX1133 was dissolved in 100% DMSO and aliquoted for storage at –20°C. For in vivo injections, mice were treated with vehicle consisting of 10% SBE-β-CD (MedChemExpress) in 50 mM citrate buffer (pH 5.0) or MRTX1133 dissolved in vehicle at 30 mg/kg dose.

Human cell lines

Human PDAC cell lines were sourced from the Institute for Applied Cancer Science (IACS) cell bank at MD Anderson Cancer Center and from ATCC. The $KRAS^{G12D}$ pancreatic cell lines AsPC1 (cultured in RPMI-1640 + 10% FBS), Panc 05.02 (cultured in RPMI-1640 + 10% FBS), and Panc 10.05 (cultured in RPMI-1640 + 15% FBS + 10 U/mL human recombinant insulin) were used. Cell lines were cultured with an additional penicillin–streptomycin (Gibco 15140122). All cell lines passed cell banking authentication and mycoplasma testing.

Data availability

RNA sequencing data for Kras* on/off iKPCs and CAF1 were deposited in GEO with accession number GSE240232.

Statistical analysis

Statistical analyses were performed using the unpaired Student's *t*-test, one-way ANOVA, two-way ANOVA, or paired multiple *t*-test depending on the experimental conditions and as shown in the figures as follows: $P < 0.05$ (*), $P < 0.01$ (**), $P < 0.001$ (***), and $P < 0.0001$ (****). For survival analyses, Kaplan–Meier survival curves were statistically analyzed by log rank (Mantel–Cox) test in GraphPad Prism 9.

Competing interest statement

R.A.D. holds equity as a founder and former advisor and/or director of Tvardi Therapeutics, Asylia Therapeutics, and Sporos Bioventures. The work of this study does not relate to the focus of these entities.

Acknowledgments

We thank Ilyas Kose, Shaolin Mei, Daniel Frigo, Jian Hu, and all members of the DePinho laboratory for helpful discussions. We thank Shan Jiang for mouse colony management and technical support on mouse work. The study made use of MD Anderson Cancer Center's Functional Genomics Core and the Advanced Cytometry and Sorting Core Facility supported by National Cancer Institute grant P30 CA016672. J.H. is supported by an Andrew Sowell-Wade Huggins Scholarship in Cancer Research. K.A.L. is supported by the Cancer Prevention and Research Institute of Texas Research Training Program (RP210028). This work was supported by National Institutes of Health grant P01 CA117969 to R.A.D. This work was also supported in part by Break Through Cancer and the Lustgarten Foundation for Pancreatic Cancer Research.

Author contributions: J.H. and R.A.D. designed the project and analyzed the data. J.H. and J.X. conducted the experiments. Y.L., K.A.L., D.C., and Y.X. assisted with experimental design and data interpretation. S.L. provided expert statistical analysis and performed normalization on public RNA-seq data sets. D.J.S., R.A.D., and J.H. reviewed the data and wrote and edited the manuscript.

References

Ambrogio C, Köhler J, Zhou ZW, Wang H, Paranal R, Li J, Capelletti M, Caffarra C, Li S, Lv Q, et al. 2018. KRAS dimerization impacts MEK inhibitor sensitivity and oncogenic activity of mutant KRAS. *Cell* **172:** 857–868.e15. doi:10.1016/J.CELL.2017.12.020

Awad MM, Liu S, Rybkin II, Arbour KC, Dilly J, Zhu VW, Johnson ML, Heist RS, Patil T, Riely GJ, et al. 2021. Acquired resistance to $KRAS^{G12C}$ inhibition in cancer. *N Engl Jo Med* **384:** 2382–2393. doi:10.1056/nejmoa2105281

Baselga J, Swain SM. 2009. Novel anticancer targets: revisiting ERBB2 and discovering ERBB3. *Nat Rev Cancer* **9:** 463–475. doi:10.1038/nrc2656

Brown WS, McDonald PC, Nemirovsky O, Awrey S, Chafe SC, Schaeffer DF, Li J, Renouf DJ, Stanger BZ, Dedhar S. 2020. Overcoming adaptive resistance to KRAS and MEK inhibitors by co-targeting mTORC1/2 complexes in pancreatic cancer. *Cell Rep Medi* **1:** 100131. doi:10.1016/J.XCRM.2020.100131

Burgess MR, Hwang E, Mroue R, Bielski CM, Wandler AM, Huang BJ, Firestone AJ, Young A, Lacap JA, Crocker L, et al. 2017. KRAS allelic imbalance enhances fitness and modulates MAP kinase dependence in cancer. *Cell* **168:** 817–829.e15. doi:10.1016/J.CELL.2017.01.020

Canon J, Rex K, Saiki AY, Mohr C, Cooke K, Bagal D, Gaida K, Holt T, Knutson CG, Koppada N, et al. 2019. The clinical $KRAS^{G12C}$ inhibitor AMG 510 drives anti-tumour immunity. *Nature* **575:** 217–223. doi:10.1038/s41586-019-1694-1

Dominguez SL, Hegde GV, Hanson JE, Xiang H, Mandikian D, Boswell CA, Chiu C, Wu Y, Tsai SP, Fleck D, et al. 2018. Antibody-mediated stabilization of NRG1 induces behavioral and electrophysiological alterations in adult mice. *Sci Rep* **8:** 94010. doi:10.1038/S41598-018-26492-4

Gulay KCM, Zhang X, Pantazopoulou V, Patel J, Esparza E, Pran Babu DS, Ogawa S, Weitz J, Ng I, Mose ES, et al. 2023. Dual inhibition of $KRAS^{G12D}$ and pan-ERBB is synergistic in pancreatic ductal adenocarcinoma. *Cancer Res* **83:** 3001–3012. doi:10.1158/0008-5472.CAN-23-1313

Gulhati P, Schalck A, Jiang S, Shang X, Wu C-J, Hou P, Ruiz SH, Soto LS, Parra E, Ying H, et al. 2023. Targeting T cell checkpoints 41BB and LAG3 and myeloid cell CXCR1/CXCR2 results in antitumor immunity and durable response in pancreatic cancer. *Nat Cancer* **4:** 62–80. doi:10.1038/s43018-022-00500-z

Hallin J, Engstrom LD, Hargi L, Calinisan A, Aranda R, Briere DM, Sudhakar N, Bowcut V, Baer BR, Ballard JA, et al. 2020. The $KRAS^{G12C}$ inhibitor MRTX849 provides insight toward therapeutic susceptibility of KRAS-mutant cancers in mouse models and patients. *Cancer Discov* **10:** 54–71. doi:10.1158/2159-8290.cd-19-1167

Hallin J, Bowcut V, Calinisan A, Briere DM, Hargis L, Engstrom LD, Laguer J, Medwid J, Vanderpool D, Lifset E, et al. 2022. Anti-tumor efficacy of a potent and selective non-covalent $KRAS^{G12D}$ inhibitor. *Nat Med* **28:** 2171–2182. doi:10.1038/s41591-022-02007-7

Heining C, Horak P, Uhrig S, Codo PL, Klink B, Hutter B, Fröhlich M, Bonekamp D, Richter D, Steiger K, et al. 2018. NRG1 fusions in KRAS wild-type pancreatic cancer. *Cancer Discov* **8:** 1087–1095. doi:10.1158/2159-8290.cd-18-0036

Hou P, Kapoor A, Zhang Q, Li J, Wu C-J, Li J, Lan Z, Tang M, Ma X, Ackroyd JJ, et al. 2020. Tumor microenvironment remodeling enables bypass of oncogenic KRAS dependency in pancreatic cancer. *Cancer Discov* **10:** 1058–1077. doi:10.1158/2159-8290.cd-19-0597

Hynes NE, Lane HA. 2005. ERBB receptors and cancer: the complexity of targeted inhibitors. *Nat Rev Cancer* **5:** 341–354. doi:10.1038/nrc1609

Ischenko I, D'Amico S, Rao M, Li J, Hayman MJ, Powers S, Petrenko O, Reich NC. 2021. KRAS drives immune evasion in a genetic model of pancreatic cancer. *Nat Commun* **12:** 1–15. doi:10.1038/s41467-021-21736-w

Kamerkar S, LeBleu VS, Sugimoto H, Yang S, Ruivo CF, Melo SA, Lee JJ, Kalluri R. 2017. Exosomes facilitate therapeutic targeting of oncogenic KRAS in pancreatic cancer. *Nature* **546:** 498–503. doi:10.1038/nature22341

Kapoor A, Yao W, Ying H, Hua S, Liewen A, Wang Q, Zhong Y, Wu C-J, Sadanandam A, Hu B, et al. 2014. Yap1 activation enables bypass of oncogenic Kras addiction in pancreatic cancer. *Cell* **158:** 185–197. doi:10.1016/j.cell.2014.06.003

Kim D, Herdeis L, Rudolph D, Zhao Y, Böttcher J, Vides A, Ayala-Santos CI, Pourfarjam Y, Cuevas-Navarro A, Xue JY, et al. 2023. Pan-KRAS inhibitor disables oncogenic signalling and tumour growth. *Nature* **619:** 160–166. doi:10.1038/s41586-023-06123-3

Little AS, Balmanno K, Sale MJ, Newman S, Dry JR, Hampson M, Edwards PAW, Smith PD, Cook SJ. 2011. Amplification of the driving oncogene, *KRAS* or *BRAF*, underpins acquired resistance to MEK1/2 inhibitors in colorectal cancer cells. *Sci Signal* **4:** ra17. doi:10.1126/scisignal.2001752

Muzumdar MD, Chen PY, Dorans KJ, Chung KM, Bhutkar A, Hong E, Noll EM, Sprick MR, Trumpp A, Jacks T. 2017. Survival of pancreatic cancer cells lacking KRAS function. *Nat Commun* **8:** 1090. doi:10.1038/s41467-017-00942-5

Pettazzoni P, Viale A, Shah P, Carugo A, Ying H, Wang H, Genovese G, Seth S, Minelli R, Green T, et al. 2015. Genetic events that limit the efficacy of MEK and RTK inhibitor therapies in a mouse model of KRAS-driven pancreatic cancer. *Cancer Res* **75:** 1091–1101. doi:10.1158/0008-5472.CAN-14-1854

Sun C, Hobor S, Bertotti A, Zecchin D, Huang S, Galimi F, Cottino F, Prahallad A, Grernrum W, Tzani A, et al. 2014. Intrinsic resistance to MEK inhibition in KRAS mutant lung and colon cancer through transcriptional induction of ERBB3. *Cell Rep* **7:** 86–93. doi:10.1016/j.celrep.2014.02.045

Tanaka N, Lin JJ, Li C, Ryan MB, Zhang J, Kiedrowski LA, Michel AG, Syed MU, Fella KA, Sakhi M, et al. 2021. Clinical acquired resistance to $KRAS^{G12C}$ inhibition through a novel KRAS switch-ii pocket mutation and polyclonal alterations converging on RAS–MAPK reactivation. *Cancer Discov* **11:** 1913–1922. doi:10.1158/2159-8290.cd-21-0365

Topham JT, Tsang ES, Karasinska JM, Metcalfe A, Ali H, Kalloger SE, Csizmok V, Williamson LM, Titmuss E, Nielsen K, et al. 2022. Integrative analysis of KRAS wildtype metastatic pancreatic ductal adenocarcinoma reveals mutation and expression-based similarities to cholangiocarcinoma. *Nat Commun* **13:** 1–13. doi:10.1038/s41467-022-33718-7

Wang X, Allen S, Blake JF, Bowcut V, Briere DM, Calinisan A, Dahlke JR, Fell JB, Fischer JP, Gunn RJ, et al. 2022. Identification of MRTX1133, a noncovalent, potent, and selective $KRAS^{G12D}$ inhibitor. *J Med Chem* **65:** 3123–3133. doi:10.1021/acs.jmedchem.1c01688

Xue JY, Zhao Y, Aronowitz J, Mai TT, Vides A, Qeriqi B, Kim D, Li C, de Stanchina E, Mazutis L, et al. 2020. Rapid non-uniform adaptation to conformation-specific $KRAS^{G12C}$ inhibition. *Nature* **577:** 421–425. doi:10.1038/S41586-019-1884-X

Ying H, Kimmelman AC, Lyssiotis CA, Hua S, Chu GC, Fletcher-Sananikone E, Locasale JW, Son J, Zhang H, Coloff JL, et al. 2012. Oncogenic Kras maintains pancreatic tumors through regulation of anabolic glucose metabolism. *Cell* **149:** 656–670. doi:10.1016/j.cell.2012.01.058